

Fig. 19. Radiograms of a metronome.

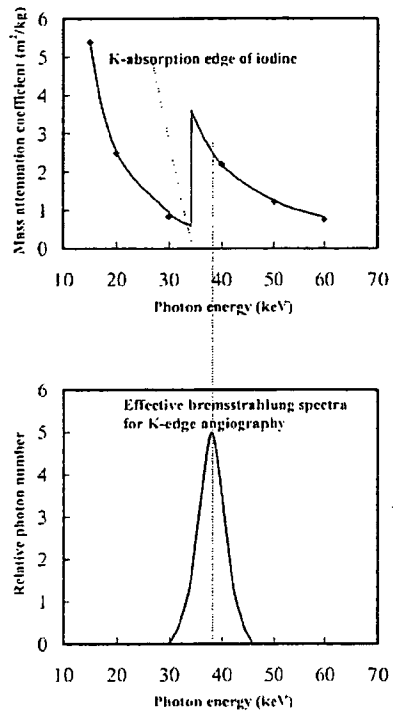


Fig. 20. Mass attenuation coefficients of iodine and effective bremsstrahlung x-rays for enhanced K-edge angiography.

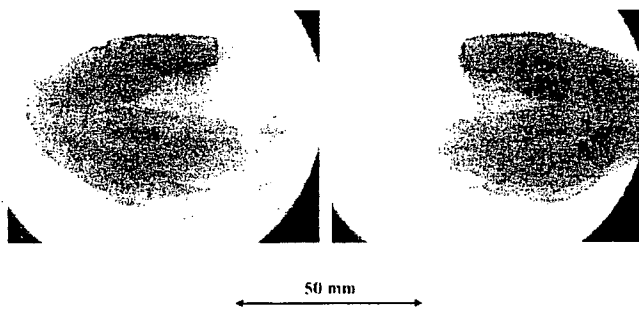


Fig. 21. Angiogram of an extracted dog heart using iodine microspheres on a tum table.

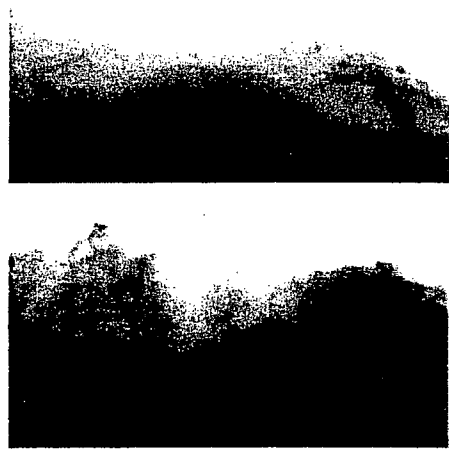


Fig. 22. Angiograms of a rabbit cancer using a high-resolution II.

## 7. CONCLUSION AND OUTLOOK

We have developed various x-ray generators corresponding to specific radiographic objectives, and the x-ray duration ranges from approximately 100 ns to continuous exposure. In the weakly ionized plasma formation, extremely clean and intense K lines were produced, since the bremsstrahlung x-rays were absorbed effectively by the plasma. In particular, the harmonic bremsstrahlung rays survived and waved due to the x-ray resonance in the plasma.

Although most flash x-ray generators utilize Marx surge generators and produce hard bremsstrahlung x-rays, monochromatic flash x-ray generators have been employed to observe aluminum grains in studies on space debris on the earth. In addition, because the monochromatic tubes realize uniform monochromatic x-ray intensity distributions, the absorber thickness can be calculated easily.

To perform enhanced K-edge angiography using iodine-based contrast media, the cerium, samarium and gadolinium targets are very useful because K lines from these targets are absorbed effectively by iodine media. Therefore, using the x-ray II in conjunction with the MLX camera with short capture times of approximately 1 ms, stop-motion images of fine blood vessels can be almost seen. Using this image intensifying system, the image quality slightly fell with decreases in the capture time. However, stop-motion image can be obtained when the capture time is decreased.

We employed an x-ray generator with a 100- $\mu\text{m}$ -focus tungsten tube and performed real-time twofold magnification radiography (fluoroscopy) using the I I and the MLX camera. To perform angiography, we employed narrow-photon-energy bremsstrahlung x-rays with a peak photon energy of approximately 35 keV, which can be absorbed easily by iodine-based contrast media. Although we obtained mostly absorption-contrast images, the phase-contrast effect may be added in cases where low-density media are employed.

Because the focus diameter of the tube has been decreased to 10  $\mu\text{m}$  using a rotating anode microfocus tube developed by Hitachi Medical Corporation, a high-resolution and high-speed magnification radiography system will become possible.

## ACKNOWLEDGMENTS

This work was supported by Grants-in-Aid for Scientific Research (13470154, 13877114, and 16591222) and Advanced Medical Scientific Research from MECSS, Health and Labor Sciences Research Grants (RAMT-nano-001, RHGTEFB-genome-005 and RHGTEFB-saisei-003), and grants from the Keiryō Research Foundation, Promotion and Mutual Aid Corporation for Private Schools of Japan, Japan Science and Technology Agency (JST), and New Energy and Industrial Technology Development Organization (NEDO, Industrial Technology Research Grant Program in '03).

## REFERENCES

1. R. Germer, "X-ray flash techniques," *J. Phys. E: Sci. Instrum.*, **12**, 336-350, 1979.
2. E. Sato, S. Kimura, S. Kawasaki, H. Isobe, K. Takahashi, Y. Tamakawa and T. Yanagisawa, "Repetitive flash x-ray generator utilizing a simple diode with a new type of energy-selective function," *Rev. Sci. Instrum.*, **61**, 2343-2348, 1990.
3. A. Shikoda, E. Sato, M. Sagae, T. Oizumi, Y. Tamakawa and T. Yanagisawa, "Repetitive flash x-ray generator having a high-durability diode driven by a two-cable-type line pulser," *Rev. Sci. Instrum.*, **65**, 850-856, 1994.
4. E. Sato, K. Takahashi, M. Sagae, S. Kimura, T. Oizumi, Y. Hayasi, Y. Tamakawa and T. Yanagisawa, "Sub-kilohertz flash x-ray generator utilizing a glass-enclosed cold-cathode triode," *Med. & Biol. Eng. & Comput.*, **32**, 289-294, 1994.
5. K. Takahashi, E. Sato, M. Sagae, T. Oizumi, Y. Tamakawa and T. Yanagisawa, "Fundamental study on a long-duration flash x-ray generator with a surface-discharge triode," *Jpn. J. Appl. Phys.*, **33**, 4146-4151, 1994.
6. E. Sato, Y. Hayasi and Y. Tamakawa, "Recent stroboscopic x-ray generators and their applications to high-speed radiography," *Ann. Rep. Iwate Med. Univ. Lib. Arts and Sci.*, **35**, 1-11, 2000.
7. E. Sato, E. Tanaka, H. Mori, T. Kawai, S. Sato, H. Ojima, K. Takayama and H. Ido, "Energy selective high-speed radiography utilizing stroboscopic x-ray generator," *SPIE*, **5580**, 765-771, 2005.
8. E. Sato, Y. Hayasi, R. Germer, K. Kimura, E. Tanaka, H. Mori, T. Kawai, T. Inoue, A. Ogawa, S. Sato, K. Takayama and H. Ido, "Energy-selective gadolinium angiography utilizing a stroboscopic x-ray generator," *SPIE*, **5920**, 59200V-1-8, 2005.

9. E. Sato, K. Sato and Y. Tamakawa, "Film-less computed radiography system for high-speed imaging," *Ann. Rep. Iwate Med. Univ. Sch. Lib. Arts and Sci.*, **35**, 13-23, 2000.
  10. E. Sato, Y. Hayasi, R. Germer, E. Tanaka, H. Mori, T. Kawai, T. Ichimaru, K. Takayama and H. Ido, "Quasi-monochromatic flash x-ray generator utilizing weakly ionized linear copper plasma," *Rev. Sci. Instrum.*, **74**, 5236-5240, 2003.
  11. E. Sato, Y. Hayasi, R. Germer, E. Tanaka, H. Mori, T. Kawai, T. Ichimaru, S. Sato, K. Takayama and H. Ido, "Sharp characteristic x-ray irradiation from weakly ionized linear plasma," *J. Electron Spectrosc. Related Phenom.*, **137-140**, 713-720, 2004.
  12. E. Sato, M. Sagae, E. Tanaka, Y. Hayasi, R. Germer, H. Mori, T. Kawai, T. Ichimaru, S. Sato, K. Takayama and H. Ido, "Quasi-monochromatic flash x-ray generator utilizing a disk-cathode molybdenum tube," *Jpn. J. Appl. Phys.*, **43**, 7324-7328, 2004.
  13. E. Sato, E. Tanaka, H. Mori, T. Kawai, S. Sato and K. Takayama, "Clean monochromatic x-ray irradiation from weakly ionized linear copper plasma," *Opt. Eng.*, **44**, 049002-1-6, 2005.
  14. E. Sato, E. Tanaka, H. Mori, T. Kawai, T. Ichimaru, S. Sato, K. Takayama and H. Ido, "Compact monochromatic flash x-ray generator utilizing a disk-cathode molybdenum tube," *Med. Phys.*, **32**, 49-54, 2005.
  15. E. Sato, Y. Hayasi, R. Germer, E. Tanaka, H. Mori, T. Kawai, T. Inoue, A. Ogawa, S. Sato, T. Ichimaru, K. Takayama, J. Onagawa and H. Ido, "Monochromatic flash x-ray generator utilizing a disk-cathode silver tube," *Opt. Eng.*, **44**, 096501-1-6, 2005.
  16. E. Sato, Y. Hayasi, K. Kimura, E. Tanaka, H. Mori, T. Kawai, T. Inoue, A. Ogawa, S. Sato, K. Takayama, J. Onagawa and H. Ido, "Enhanced K-edge angiography utilizing tantalum plasma x-ray generator in conjunction with gadolinium-based contrast media," *Jpn. J. Appl. Phys.*, **44**, 8716-8721, 2005.
  17. E. Sato, Y. Hayasi, R. Germer, K. Kimura, E. Tanaka, H. Mori, T. Kawai, T. Inoue, A. Ogawa, S. Sato, K. Takayama and H. Ido, "Enhanced K-edge plasma angiography achieved with tungsten Ka rays utilizing gadolinium-based contrast media," *SPIE*, **5920**, 592012-1-8, 2005.
  18. E. Sato, Y. Hayasi, R. Germer, E. Tanaka, H. Mori, T. Kawai, T. Inoue, A. Ogawa, S. Sato, K. Takayama, J. Onagawa, "X-ray spectra from weakly ionized linear copper plasma," *Jpn. J. Appl. Phys.*, **45**, 5301-5306, 2006.
  19. E. Sato, E. Tanaka, H. Mori, T. Kawai, T. Ichimaru, S. Sato, K. Takayama and H. Ido, "Demonstration of enhanced K-edge angiography using a cerium target x-ray generator," *Med. Phys.*, **31**, 3017-3021, 2004.
  20. E. Sato, A. Yamadera, E. Tanaka, H. Mori, T. Kawai, F. Ito, T. Inoue, A. Ogawa, S. Sato, K. Takayama, J. Onagawa and H. Ido, "X-ray spectra from a cerium target and their application to cone beam K-edge angiography," *Opt. Eng.*, **44**, 096502-1-6, 2005.
  21. E. Sato, E. Tanaka, H. Mori, T. Kawai, T. Inoue, A. Ogawa, A. Yamadera, S. Sato, F. Ito, K. Takayama, J. Onagawa and H. Ido, "Variations in cerium x-ray spectra and enhanced K-edge angiography," *Jpn. J. Appl. Phys.*, **44**, 8204-8209, 2005.
  22. E. Sato, E. Tanaka, H. Mori, H. Kawakami, T. Kawai, T. Inoue, A. Ogawa, S. Sato, T. Ichimaru, K. Takayama and H. Ido, "Enhanced magnification angiography including phase-contrast effect using a 100- $\mu\text{m}$  focus x-ray tube," *SPIE*, **5918**, 591811-1-9, 2005.
- \*dresato@iwate-med.ac.jp; phone +81-19-651-5111; fax +81-19-654-9282

# High-sensitive radiography system utilizing a pulse x-ray generator and a night-vision CCD camera (MLX)

Eiichi Sato\*<sup>a</sup>, Michiaki Sagae<sup>a</sup>, Etsuro Tanaka<sup>b</sup>, Hidezo Mori<sup>c</sup>, Toshiaki Kawai<sup>d</sup>, Takashi Inoue<sup>e</sup>, Akira Ogawa<sup>e</sup>, Shigehiro Sato<sup>f</sup>, Toshio Ichimaru<sup>g</sup> and Kazuyoshi Takayama<sup>h</sup>

<sup>a</sup>Department of Physics, Iwate Medical University, 3-16-1 Honchodori, Morioka 020-0015, Japan,

<sup>b</sup>Department of Nutritional Science, Faculty of Applied Bio-science, Tokyo University of Agriculture, 1-1-1 Sakuragaoka, Setagaya-ku 156-8502, Japan

<sup>c</sup>Department of Cardiac Physiology, National Cardiovascular Center Research Institute, 5-7-1 Fujishirodai, Suita, Osaka 565-8565 Japan

<sup>d</sup>Electron Tube Division #2, Hamamatsu Photonics Inc., 314-5 Shimokanzo, Iwata 438-0193, Japan

<sup>e</sup>Department of Neurosurgery, School of Medicine, Iwate Medical University, 19-1 Uchimaru, Morioka 020-8505, Japan

<sup>f</sup>Department of Microbiology, School of Medicine, Iwate Medical University, 19-1 Uchimaru, Morioka 020-8505, Japan

<sup>g</sup>Department of Radiological Technology, School of Health Sciences, Hirosaki University, 66-1 Honcho, Hirosaki 036-8564, Japan

<sup>h</sup>Tohoku University Biomedical Engineering Research Organization, 2-1-1 Katahira, Sendai 980-8577, Japan

## ABSTRACT

High-sensitive radiography system utilizing a kilohertz-range stroboscopic x-ray generator and a night-vision CCD camera (MLX) is described. The x-ray generator consists of the following major components: a main controller, a condenser unit with a Cockcroft-Walton circuit, and an x-ray tube unit in conjunction with a grid controller. The main condenser of about 500 nF in the unit is charged up to 100 kV by the circuit, and the electric charges in the condenser are discharged to the triode by the grid control circuit. The maximum tube current and the repetition rate are approximately 0.5 A and 50 kHz, respectively. The x-ray pulse width ranges from 0.01 to 1.0 ms, and the maximum shot number has a value of 32. At a charging voltage of 60 kV and a width of 1.0 ms, the x-ray intensity obtained without filtering was 6.04  $\mu$ Gy at 1.0 m per pulse. In radiography, an object is exposed by the pulse x-ray generator, and a radiogram is taken by an image intensifier. The image is intensified by the CCD camera, and a stop-motion image is stored by a flash memory device using a trigger delay device. The image quality was improved with increases in the x-ray duration, and a single-shot radiography was performed with durations of less than 1.0 ms.

**Keywords:** high-sensitive radiography, image intensification, high-sensitive CCD camera, pulse x-ray generator

## 1. INTRODUCTION

With advances in high-voltage pulse technology, high-photon-energy flash x-ray generators<sup>1,2</sup> have been developed utilizing multi-stage Marx generators, and the maximum photon energy has been increased up to approximately 1 MeV for military applications. In contrast, we have developed low-photon-energy flash x-ray generators<sup>3-6</sup> with photon energies of lower than 150 keV, and have performed high-speed soft radiographies including biomedical applications.

To produce extremely clean K-series characteristic x-rays such as lasers, we have developed three characteristic flash x-ray generators<sup>7-15</sup> and have succeeded in producing clean K lines. In particular, bremsstrahlung x-rays are absorbed effectively by weakly ionized metal plasmas. Subsequently, we have developed steady-state characteristic x-ray

generators<sup>16</sup> and have succeeded in producing clean K lines utilizing angle dependence of the bremsstrahlung x-rays. In the biomedical field, because there are no ultra-high-speed movements, a condenser-discharge stroboscopic x-ray generator<sup>17,18</sup> has been developed. In this generator, the x-ray duration can be controlled from 10  $\mu$ s to 1.0 ms, and the maximum repetition rate is approximately 50 kHz. In conjunction with a computed radiography (CR) system, short-duration and multi-shot radiographies are possible. In addition, the velocity of a high-speed object can be calculated easily by measuring the length of blurring because the x-ray duration can be controlled correctly within 1.0 ms.

Recently, because an extremely high-sensitive color CCD camera (MLX) has been developed by NAC image technology, we are very interested in intensifying the x-ray image signals using the MLX camera in conjunction with a pulse x-ray generator. Using image intensifying, the absorbed dose can be reduced from patients.

In this research, we employed a stroboscopic x-ray generator and performed a preliminary study on the intensification of image signal, utilizing an image intensifier and the high-sensitive CCD camera.

## 2. PULSE X-RAY GENERATOR

Figure 1 shows the block diagram of a kilohertz-range stroboscopic x-ray generator. This generator consists of the following major components: a main controller, a condenser unit with a Cockcroft-Walton circuit, and an x-ray tube unit in conjunction with a grid controller. The main condenser of about 500 nF in the unit is charged up to 100 kV by the circuit, and the electric charges in the condenser are discharged to the triode by the grid control circuit. Although the tube voltage decreased during the discharging for generating x-rays, the maximum value was equal to the initial charging voltage of the main condenser.

The x-ray tube is a glass-enclosed hot-cathode triode and is composed of the following major parts: an anode rod made of copper, a tungsten plate target, an iron focusing electrode, a tungsten hot cathode (filament), a tungsten grid, and a glass tube body. The electron beams from the cathode are accelerated between the anode and cathode electrodes and are converged to the target by the focusing electrode. The tube is set in the metal case filled with insulation oil, and the diaphragm regulates the irradiation field.

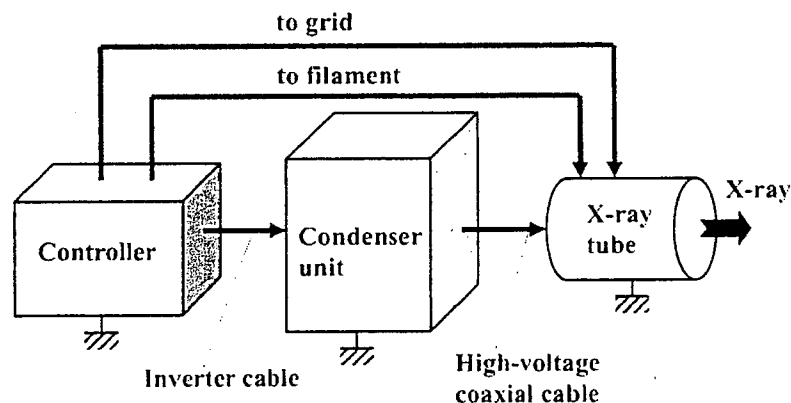


Fig. 1. Block diagram of the kilohertz-range stroboscopic x-ray generator.

## 3. CHARACTERISTICS

### 3.1 X-ray output

The x-ray output was detected by a pin diode, and the output voltages from the diode were measured by a digital storage scope (Fig. 2). When the charging voltage was increased, the pulse height increased substantially. Using this generator, the pulse width can be controlled correctly and ranged from 10  $\mu$ s to 1.0 ms. The maximum repetition rate was approximately 50 kHz, and stable repetitive x-ray pulses were obtained.

### 3.2 Time-integrated x-ray intensity

Figure 3 shows the time-integrated (absolute) value of the x-ray intensity at 1.0 m per pulse measured by a Victoreen 660 ionization chamber. The intensity was proportional to the x-ray duration. At a constant pulse width of 1.0 ms, the intensity increased with increasing the charging voltage. At a charging voltage of 60 kV and a width of 1.0 ms, the x-ray intensity was 6.04  $\mu\text{Gy}$  per pulse at 1.0 m from the source.

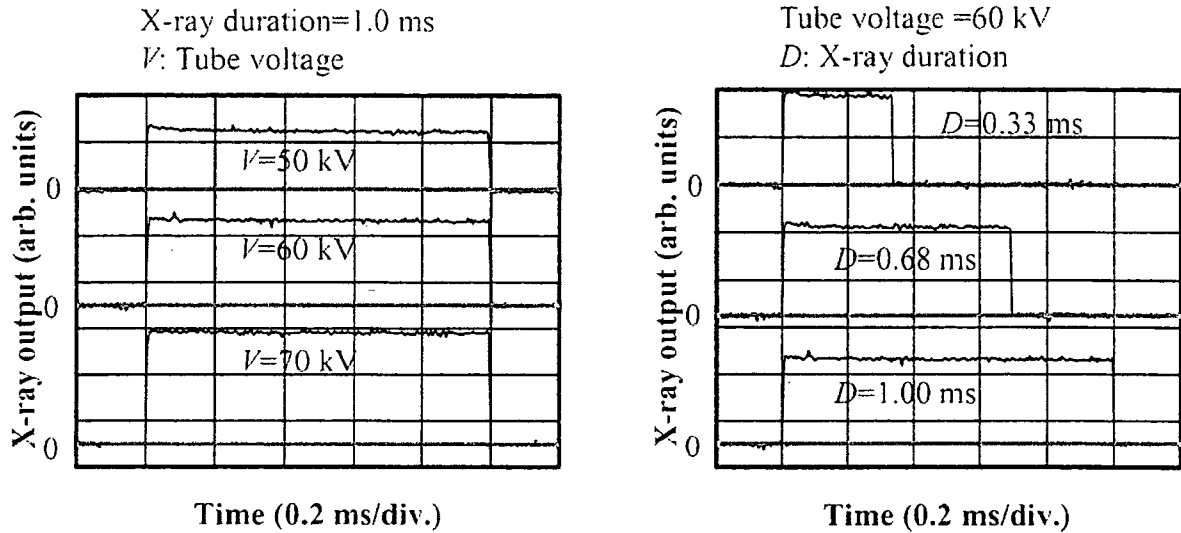


Fig. 2. X-ray outputs at indicated conditions.

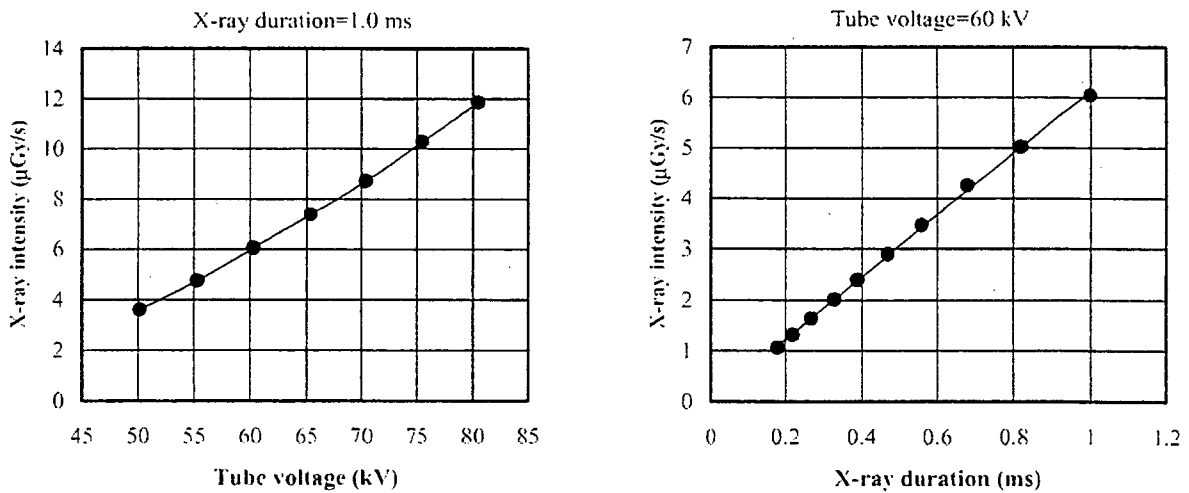


Fig. 3. X-ray intensities at 1.0 m from the x-ray source.

#### 4. RADIOGRAPHY

Figure 4 shows the experimental setup for intensifying x-ray image signals using the MLX camera. An object is exposed by the pulse x-ray generator, and a radiogram is taken by an image intensifier. Then, the image is amplified by the CCD camera, and a stop-motion image is stored by a flash memory device using a trigger delay device with a delay time of 50 ms. The image quality improved with increases in the x-ray duration, and single-shot radiography was performed with durations of less than 1.0 ms.

First, rough measurements of spatial resolution were made using wires. Figure 5 shows a radiogram of a 200- $\mu\text{m}$ -diameter tungsten wire coiled around a pipe made of polymethyl methacrylate. In this radiography, the wire was observed with blurring, and image quality improved with increases in the x-ray duration. Next, two radiograms of a metronome are shown in Fig. 6, and stop-motion images of a pendulum are visible. In radiography of plastic bullets, spherical bullets were clearly observed (Fig. 7). Finally, the image of water falling into a polypropylene beaker from a plastic test tube is shown in Fig. 8. This image was taken with the slight addition of an iodine-based contrast medium. Because the x-ray duration was 1 ms, the stop-motion image of water could be obtained.

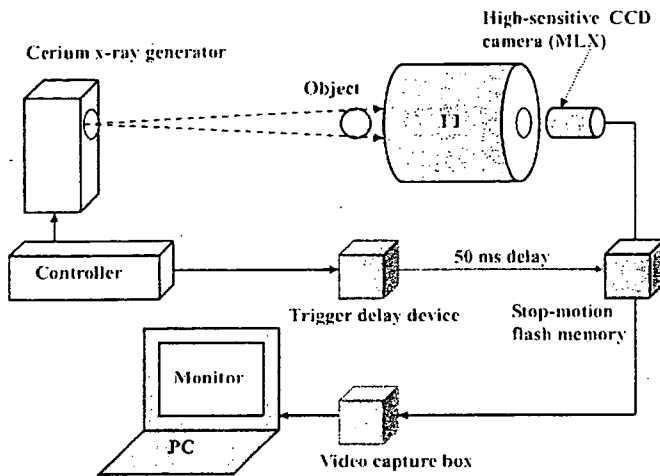


Fig. 4. Experimental setup for performing real-time radiography utilizing the MLX camera.



Fig. 5. Radiogram of a 200- $\mu\text{m}$ -diameter tungsten wire coiled around a pipe made of polymethyl methacrylate.

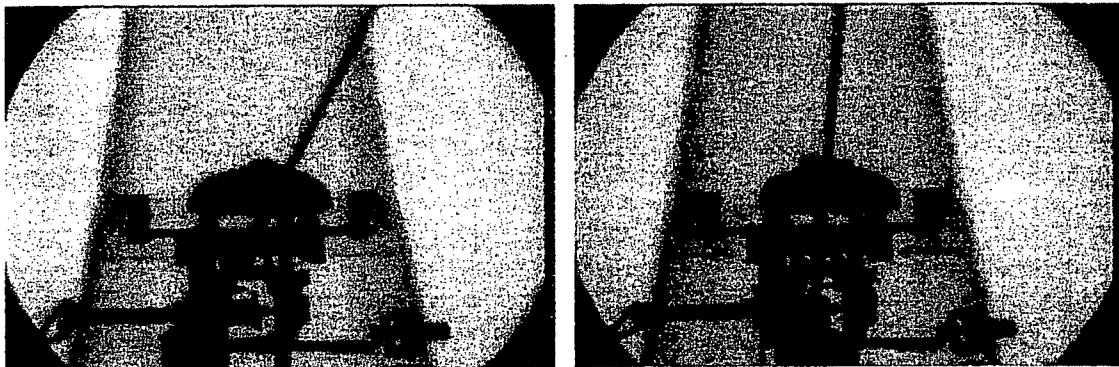


Fig. 6. Two radiograms of a metronome.

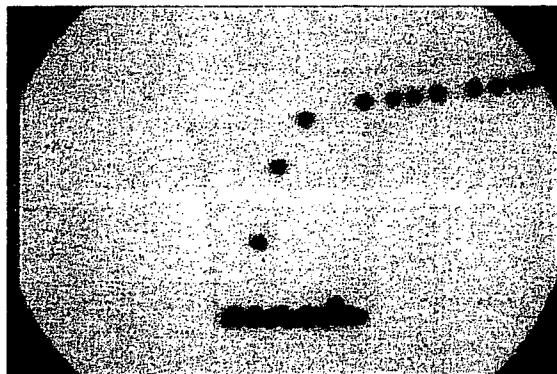


Fig. 7. Radiogram of plastic bullets falling into a polypropylene beaker from a plastic test tube.

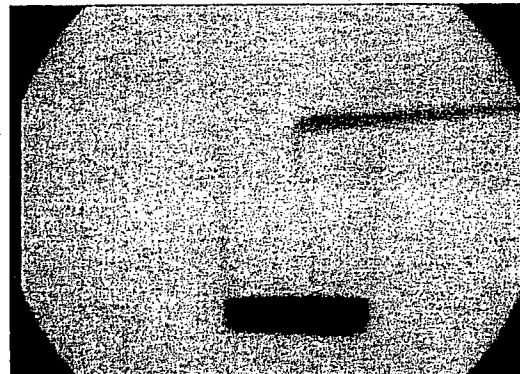


Fig. 8. Radiogram of water falling into a polypropylene beaker from a plastic test tube using an iodine medium.

## 5. DISCUSSION

We performed a fundamental study on the intensification of the x-ray image signal using the MLX camera, and the image quality improved with increases in the x-ray duration. The spatial resolution was primarily determined by the resolution of I I and the pixel number of the camera. Therefore, the resolution improves with improving the I I resolution and with increasing the pixel number.

Without considering the absorbed dose, short-duration real-time radiography is possible by decreasing the image capture time of the camera using a steady-state x-ray generator. In cases where a microfocus x-ray generator is employed, the spatial resolution improves using magnification radiography, and the real-time radiography with a capture time of 1 ms can be performed by image intensifying.

In this experiment, although we performed only single-shot radiography, high-speed dynamic radiography could be possible using a high-speed high-sensitive video camera synchronizing to the repetitive x-ray output, and the repetition rate can be increased to approximately 50 kHz.

## ACKNOWLEDGMENTS

This work was supported by Grants-in-Aid for Scientific Research (13470154, 13877114, 16591181, and 16591222) and Advanced Medical Scientific Research from MECSS, Health and Labor Sciences Research Grants (RAMT-nano-001, RHGTEFB-genome-005 and RHGTEFB-saisei-003), Grants from The Keiryō Research Foundation, The Promotion and Mutual Aid Corporation for Private Schools of Japan, Japan Science and Technology Agency (JST), and the New Energy and Industrial Technology Development Organization (NEDO, Industrial Technology Research Grant Program in '03).

## REFERENCES

1. A. Mattsson, "Some characteristics of a 600 kV flash x-ray tube," *Physica Scripta*, **5**, 99-102, 1972.
2. R. Germer, "X-ray flash techniques," *J. Phys. E: Sci. Instrum.*, **12**, 336-350, 1979.
3. E. Sato, S. Kimura, S. Kawasaki, H. Isobe, K. Takahashi, Y. Tamakawa and T. Yanagisawa, "Repetitive flash x-ray generator utilizing a simple diode with a new type of energy-selective function," *Rev. Sci. Instrum.*, **61**, 2343-2348, 1990.



4. A. Shikoda, E. Sato, M. Sagae, T. Oizumi, Y. Tamakawa and T. Yanagisawa, "Repetitive flash x-ray generator having a high-durability diode driven by a two-cable-type line pulser," *Rev. Sci. Instrum.*, **65**, 850-856, 1994.
5. E. Sato, K. Takahashi, M. Sagae, S. Kimura, T. Oizumi, Y. Hayasi, Y. Tamakawa and T. Yanagisawa, "Sub-kilohertz flash x-ray generator utilizing a glass-enclosed cold-cathode triode," *Med. & Biol. Eng. & Comput.*, **32**, 289-294, 1994.
6. K. Takahashi, E. Sato, M. Sagae, T. Oizumi, Y. Tamakawa and T. Yanagisawa, "Fundamental study on a long-duration flash x-ray generator with a surface-discharge triode," *Jpn. J. Appl. Phys.*, **33**, 4146-4151, 1994.
7. E. Sato, Y. Hayasi, R. Germer, E. Tanaka, H. Mori, T. Kawai, T. Ichimaru, K. Takayama and H. Ido, "Quasi-monochromatic flash x-ray generator utilizing weakly ionized linear copper plasma," *Rev. Sci. Instrum.*, **74**, 5236-5240, 2003.
8. E. Sato, Y. Hayasi, R. Germer, E. Tanaka, H. Mori, T. Kawai, T. Ichimaru, S. Sato, K. Takayama and H. Ido, "Sharp characteristic x-ray irradiation from weakly ionized linear plasma," *J. Electron Spectrosc. Related Phenom.*, **137-140**, 713-720, 2004.
9. E. Sato, M. Sagae, E. Tanaka, Y. Hayasi, R. Germer, H. Mori, T. Kawai, T. Ichimaru, S. Sato, K. Takayama and H. Ido, "Quasi-monochromatic flash x-ray generator utilizing a disk-cathode molybdenum tube," *Jpn. J. Appl. Phys.*, **43**, 7324-7328, 2004.
10. E. Sato, E. Tanaka, H. Mori, T. Kawai, S. Sato and K. Takayama, "Clean monochromatic x-ray irradiation from weakly ionized linear copper plasma," *Opt. Eng.*, **44**, 049002-1-6, 2005.
11. E. Sato, E. Tanaka, H. Mori, T. Kawai, T. Ichimaru, S. Sato, K. Takayama and H. Ido, "Compact monochromatic flash x-ray generator utilizing a disk-cathode molybdenum tube," *Med. Phys.*, **32**, 49-54, 2005.
12. E. Sato, Y. Hayasi, R. Germer, E. Tanaka, H. Mori, T. Kawai, T. Inoue, A. Ogawa, S. Sato, T. Ichimaru, K. Takayama, J. Onagawa and H. Ido, "Monochromatic flash x-ray generator utilizing a disk-cathode silver tube," *Opt. Eng.*, **44**, 096501-1-6, 2005.
13. E. Sato, Y. Hayasi, K. Kimura, E. Tanaka, H. Mori, T. Kawai, T. Inoue, A. Ogawa, S. Sato, K. Takayama, J. Onagawa and H. Ido, "Enhanced K-edge angiography utilizing tantalum plasma x-ray generator in conjunction with gadolinium-based contrast media," *Jpn. J. Appl. Phys.*, **44**, 8716-8721, 2005.
14. E. Sato, Y. Hayasi, R. Germer, K. Kimura, E. Tanaka, H. Mori, T. Kawai, T. Inoue, A. Ogawa, S. Sato, K. Takayama and H. Ido, "Enhanced K-edge plasma angiography achieved with tungsten K $\alpha$  rays utilizing gadolinium-based contrast media," *SPIE*, **5920**, 592012-1-8, 2005.
15. E. Sato, Y. Hayasi, R. Germer, E. Tanaka, H. Mori, T. Kawai, T. Inoue, A. Ogawa, S. Sato, K. Takayama, J. Onagawa, "X-ray spectra from weakly ionized linear copper plasma," *Jpn. J. Appl. Phys.*, **45**, 5301-5306, 2006.
16. E. Sato, E. Tanaka, H. Mori, T. Kawai, T. Inoue, A. Ogawa, S. Sato, K. Takayama and J. Onagawa, "Characteristic x-ray generator utilizing angle dependence of bremsstrahlung x-ray distribution," *Jpn. J. Appl. Phys.*, **45**, 2845-2849, 2006.
17. E. Sato, E. Tanaka, H. Mori, T. Kawai, S. Sato, H. Ojima, K. Takayama and H. Ido, "Energy selective high-speed radiography utilizing stroboscopic x-ray generator," *SPIE*, **5580**, 765-771, 2005.
18. E. Sato, Y. Hayasi, R. Germer, K. Kimura, E. Tanaka, H. Mori, T. Kawai, T. Inoue, A. Ogawa, S. Sato, K. Takayama and H. Ido, "Energy-selective gadolinium angiography utilizing a stroboscopic x-ray generator," *SPIE*, **5920**, 59200V-1-8, 2005.

\*dresato@iwate-med.ac.jp; phone +81-19-651-5111; fax +81-19-654-9282

# K-edge magnification digital angiography using a 100- $\mu\text{m}$ -focus tungsten tube

**Eiichi Sato**, MEMBER SPIE  
Iwate Medical University  
Department of Physics  
Morioka 020-0015, Japan

**Etsuro Tanaka**  
Tokyo University of Agriculture  
Department of Nutritional Science  
Faculty of Applied Bioscience  
Setagaya-ku 156-8502, Japan

**Hidezo Mori**  
National Cardiovascular Center Research Institute  
Department of Cardiac Physiology  
Osaka 565-8565, Japan

**Hiroki Kawakami**  
**Toshiaki Kawai**, MEMBER SPIE  
Hamamatsu Photonics K. K.  
Electron Tube Division 2  
Iwata 438-0193, Japan

**Takashi Inoue**  
**Akira Ogawa**  
Iwate Medical University  
Department of Neurosurgery  
School of Medicine  
Morioka 020-8505, Japan

**Mitsuru Izumisawa**  
Iwate Medical University  
Department of Oral Radiology  
School of Dentistry  
Morioka 020-0021, Japan

**Kiyomi Takahashi**  
**Shigehiro Sato**  
Iwate Medical University  
Department of Microbiology  
School of Medicine  
Morioka 020-8505, Japan

**Kazuyoshi Takayama**, MEMBER SPIE  
Tohoku University  
Shock Wave Research Center  
Institute of Fluid Science  
Sendai 980-8577, Japan

**Jun Onagawa**  
Tohoku Gakuin University  
Department of Applied Physics and Informatics  
Faculty of Engineering  
Tagajo 985-8537, Japan

**Abstract.** A microfocus x-ray tube is useful to perform magnification digital radiography, including phase-contrast effects. The 100- $\mu\text{m}$ -focus x-ray generator consists of a main controller for regulating the tube voltage and current, and a tube unit with a high-voltage circuit and a fixed anode x-ray tube. The maximum tube voltage, current, and electric power are 105 kV, 0.5 mA, and 50 W, respectively. Using a 3-mm-thick aluminum filter, the x-ray intensity is 26.0  $\mu\text{Gy/s}$  at 1.0 m from the source, with a tube voltage of 60 kV and a current of 0.50 mA. Because the peak photon energy is approximately 35 keV using the filter with a tube voltage of 60 kV, the bremsstrahlung x-rays are absorbed effectively by iodine-based contrast media with an iodine K-edge of 33.2 keV. Magnification angiography is performed by three-fold magnification imaging with a computed radiography system using iodine-based microspheres 15  $\mu\text{m}$  in diameter. In angiography of nonliving animals, we observe fine blood vessels approximately 100  $\mu\text{m}$  with high contrasts.  
© 2007 Society of Photo-Optical Instrumentation Engineers.  
[DOI: 10.1117/1.2542285]

**Subject terms:** high-contrast angiography; magnification digital radiography; microfocus x-ray tube; energy-selective imaging; phase-contrast effect.

Paper 051014R received Dec. 27, 2005; revised manuscript received Aug. 9, 2006; accepted for publication Aug. 10, 2006; published online Mar. 2, 2007. This paper is a revision of a paper presented at the SPIE conference on Laser-Generated, Synchrotron, and Other Laboratory X-Ray and EUV Sources, Optics, and Applications II, Aug. 2005, San Diego, California. The paper presented there appears (unrefereed) in SPIE Proceedings Vol. 5918.

## 1 Introduction

Conventional flash x-ray generators utilizing condensers in conjunction with cold-cathode tubes are useful to perform high-speed radiography, including biomedical applications, and several different generators have been developed.<sup>1-7</sup> In particular, linear-plasma x-ray generators<sup>8-10</sup> utilizing triodes have been employed to produce clean K-series characteristic x-rays of nickel and copper, and we have confirmed the irradiation of higher harmonic hard x-rays of K-series characteristic x-rays. Without forming plasmas, a flash x-ray diode with a disk cathode can be employed to perform a fundamental study on producing characteristic x-rays,<sup>11,12</sup> and we have succeeded in producing clean K-series lines using the angle dependence of bremsstrahlung x-ray distribution in Sommerfeld's theory. However, monochromatic flash radiography has had difficulties in increasing x-ray duration and in performing magnification radiography, including the phase-contrast effect.

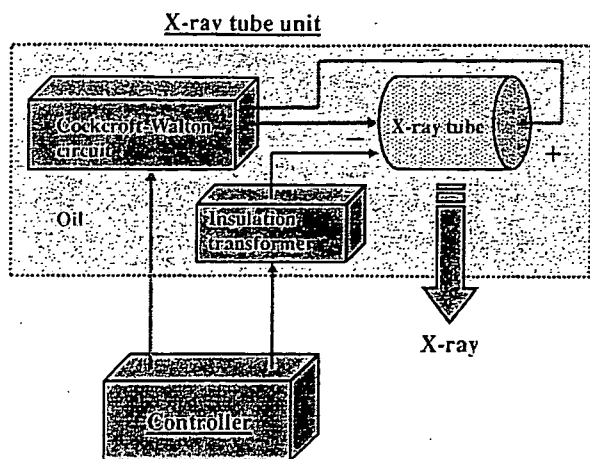


Fig. 1 Block diagram of the x-ray generator.

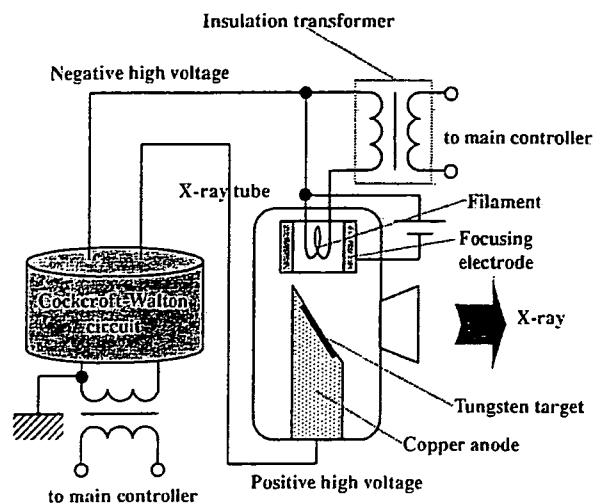


Fig. 2 Electric circuit of the x-ray generator.

Synchrotrons are capable of producing high-dose-rate monochromatic parallel x-ray beams using a monochromolimator, and the beams have been applied to phase-contrast radiography<sup>13,14</sup> and enhanced K-edge angiography.<sup>15,16</sup> In angiography, monochromatic x-rays with photon energies approximately 35 keV have been employed, because the rays are absorbed effectively by iodine-based contrast media with an iodine K edge of 33.2 keV.

Without using synchrotrons, phase-contrast radiography for edge enhancement can be performed using a microfocuss x-ray tube. Magnification radiography, including the phase-contrast effect, has been applied in mammography achieved with a computed radiography (CR) system<sup>17</sup> using a 100- $\mu\text{m}$ -focus molybdenum tube.<sup>18</sup> Subsequently, we have developed a cerium x-ray generator<sup>19,20</sup> to perform enhanced K-edge angiography using cone beams, and have succeeded in observing fine blood vessels and coronary arteries with high contrasts using cerium  $K\alpha$  rays of 34.6 keV. However, it is difficult to design a small focus cerium tube for angiography.

Magnification radiography is useful to improve the spatial resolution in digital radiography, and the phase contrast may come into effect in edge enhancement of comparatively large objects, including thick blood vessels filled with low-density contrast media. Therefore, narrow-photon-energy bremsstrahlung x-rays with a peak energy of approximately 35 keV from a microfocuss tungsten tube are useful to perform high-contrast high-resolution angiography.

In the present research, we employed a 100- $\mu\text{m}$ -focus tungsten tube, used to perform enhanced magnification angiography by controlling bremsstrahlung x-ray spectra using an aluminum filter.

## 2 Experimental Setup

Figure 1 shows the block diagram of a microfocuss x-ray generator used in this experiment, and the generator consists of a main controller, an x-ray tube unit with a Cockcroft-Walton circuit, an insulation transformer, and a 100- $\mu\text{m}$ -focus x-ray tube. The tube voltage, current, and exposure time can be controlled by the controller. The main circuit for producing x-rays is illustrated in Fig. 2, and employs the Cockcroft-Walton circuit to decrease the dimen-

sions of the tube unit. In the x-ray tube, positive and negative high voltages are applied to the anode and cathode electrodes, respectively. The filament heating current is supplied by an AC power supply in the controller, in conjunction with an insulation transformer, which is used for isolation from the high voltage from the Cockcroft-Walton circuit. In this experiment, the tube voltage applied was from 45 to 70 kV, and the tube current was regulated to within 0.50 mA (maximum current) by the filament temperature. The exposure time is controlled to obtain optimum x-ray intensity, and narrow-photon-energy bremsstrahlung x-rays are produced using a 3.0-mm-thick aluminum filter for absorbing soft x-rays.

## 3 Results and Discussion

### 3.1 X-Ray Intensity

The x-ray intensity was measured by a Victoreen 660 ionization chamber 1.0 m from the x-ray source using the filter (Fig. 3). At a constant tube current of 0.50 mA, the x-ray

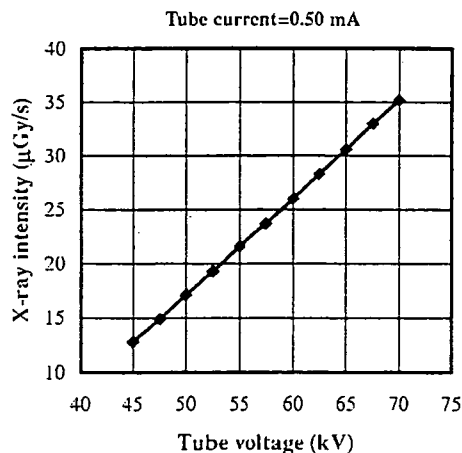


Fig. 3 X-ray intensity ( $\mu\text{Gy/s}$ ) as a function of tube voltage (kV) with a tube current of 0.50 mA.

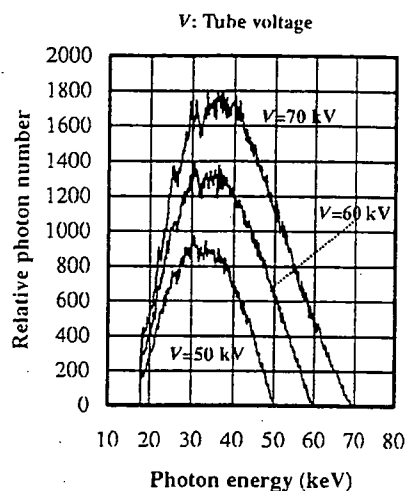


Fig. 4 Bremsstrahlung x-ray spectra measured using a cadmium telluride detector with changes in the tube voltage.

intensity increased when the tube voltage was increased. At a tube voltage of 60 kV, the intensity with the filter was  $26.0 \mu\text{Gy/s}$ .

### 3.2 X-Ray Spectra

To measure x-ray spectra, we employed a cadmium telluride detector (XR-100T, Amptek) (Fig. 4). When the tube voltage was increased, the bremsstrahlung x-ray intensity increased, and both the maximum photon energy and the spectrum peak energy increased.

To perform K-edge angiography, bremsstrahlung x-rays of approximately 35 keV are useful, and the high-energy bremsstrahlung x-rays decrease the image contrast. Using this filter, because bremsstrahlung x-rays with energies higher than 60 keV were not absorbed easily, the tube voltage for angiography was determined as 60 kV by considering the filtering effect of radiographic objects.

### 3.3 Magnification Radiography

Magnification radiography was performed by threefold magnification imaging using the CR system and the filter at a tube voltage of 60 kV. The distance between the x-ray source and the imaging plate was 1.5 m (Fig. 5). First, the spatial resolutions of conventional (cohesion) and magnification radiographies were made using a lead test chart. In the magnification radiography,  $62.5\text{-}\mu\text{m}$  lines (eight line pairs) were visible (Fig. 6). Subsequently, Fig. 7 shows radiograms of tungsten wires coiled around rods made of

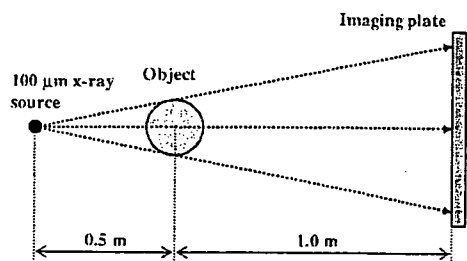


Fig. 5 Threefold magnification imaging using an imaging plate in conjunction with a microfocus tube.

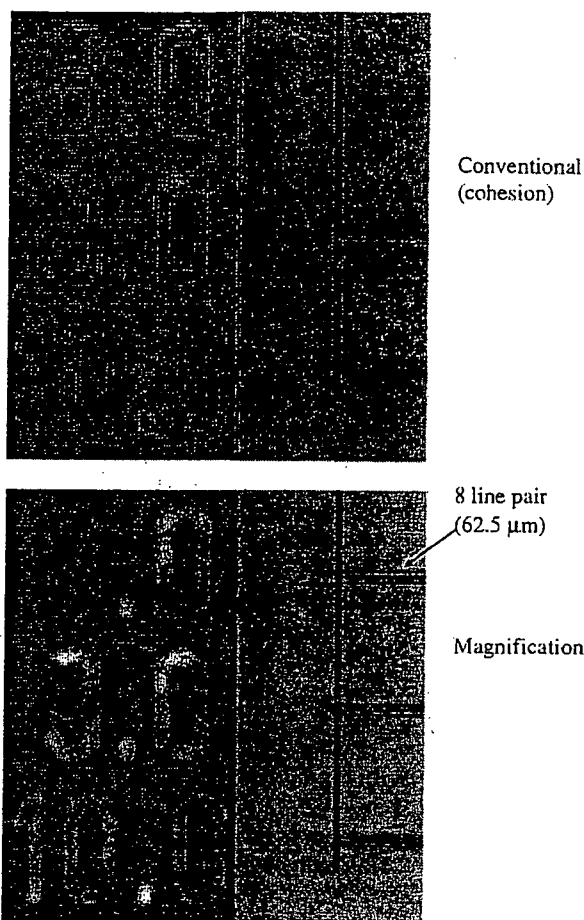


Fig. 6 Radiograms of a test chart for measuring the spatial resolution.

polymethyl methacrylate (PMMA). Although the image contrast decreased somewhat with decreases in the wire diameter, due to blurring of the image caused by the sampling pitch of  $87.5 \mu\text{m}$ , a  $50\text{-}\mu\text{m}$ -diam wire could be observed. Radiograms of one set of a bolt and a nut are shown in Fig. 8. The edge of a bubble in the bolt and the seam between the bolt and the nut are visible in magnification radiography.

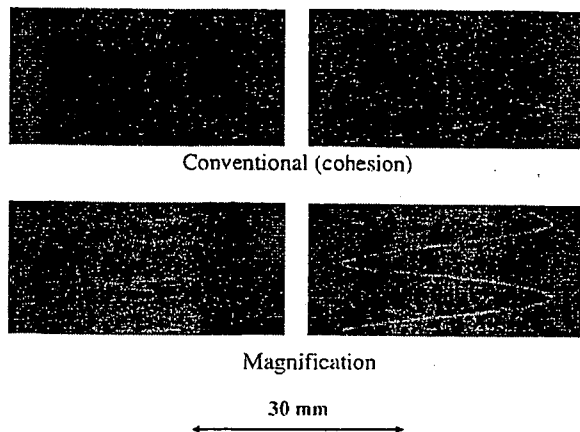


Fig. 7 Radiograms of tungsten wires coiled around PMMA rods.

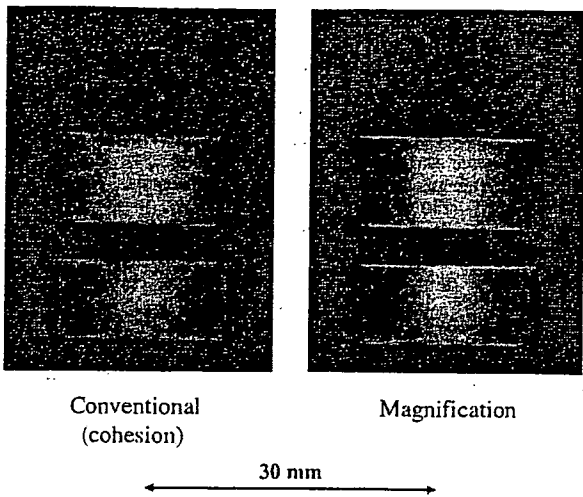


Fig. 8 Radiograms of a plastic bolt and nut.

### 3.4 Enhanced Magnification Angiography

Figure 9 shows the mass attenuation coefficients of iodine at the selected energies; the coefficient curve is discontinuous at the iodine K edge. The effective bremsstrahlung x-ray spectra for K-edge angiography are shown above the iodine K edge. Because iodine contrast media with a K-absorption edge of 33.2 keV absorb the rays easily, blood vessels were observed with high contrasts.

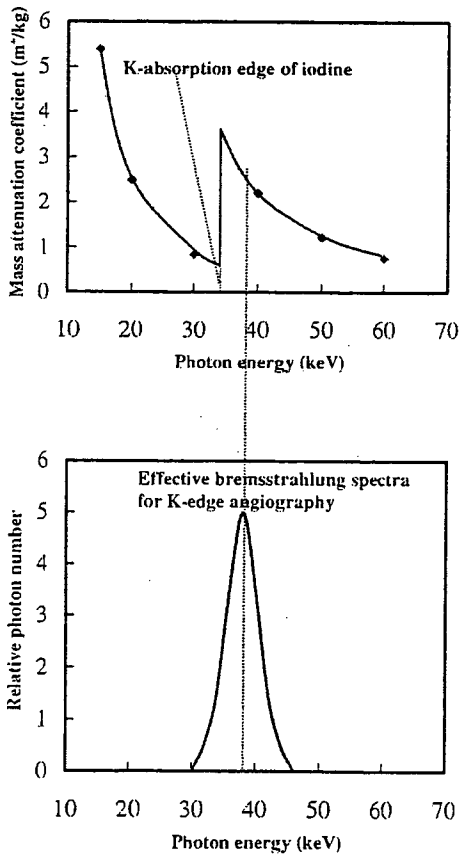


Fig. 9 Mass attenuation coefficients of iodine and effective bremsstrahlung x-rays for enhanced K-edge angiography.

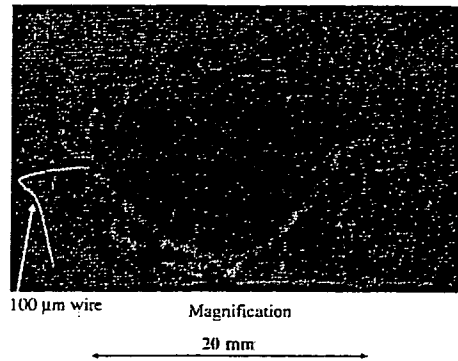


Fig. 10 Angiogram of an extracted rabbit heart using iodine microspheres.

Magnification angiography was performed at the same conditions using iodine microspheres of 15  $\mu\text{m}$  in diameter. The microspheres (containing 37% iodine by weight) are very useful for making phantoms of nonliving animals used for angiography. An angiogram of a rabbit heart is shown in Fig. 10, and the coronary arteries are visible. Figure 11 shows angiograms of a larger dog heart using iodine spheres. Although the image contrast decreased slightly with increases in the thickness of the PMMA plate facing the x-ray source, coronary arteries of approximately 100  $\mu\text{m}$  were observed using a 100-mm-thick plate.

### 4 Conclusion and Outlook

We employ an x-ray generator with a 100- $\mu\text{m}$ -focus tungsten tube and perform enhanced K-edge magnification angiography using narrow-photon-energy bremsstrahlung x-rays with a peak photon energy of approximately 35 keV, which can be absorbed easily by iodine-based contrast me-

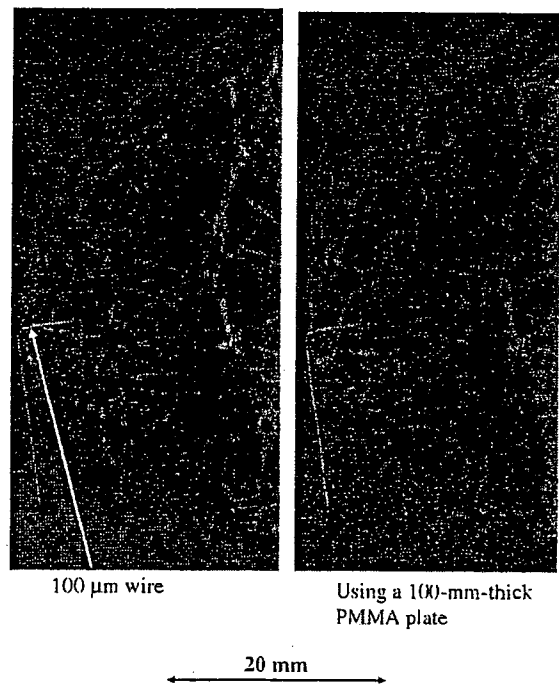


Fig. 11 Angiograms of an extracted dog heart.

dia. The bremsstrahlung x-ray intensity substantially increases with increase in the tube voltage, and the tube voltage is determined as 60 kV to increase the image contrast. In magnification angiography, although we obtain mostly absorption-contrast images, the phase-contrast effect may be added in cases where low-density media are employed.

Because the sampling pitch of the CR system is  $87.5\ \mu\text{m}$ , we obtain spatial resolutions of approximately  $50\ \mu\text{m}$  using threefold magnification imaging, even when a  $100\text{-}\mu\text{m}$ -focus tube is employed. To observe fine blood vessels of less than  $100\ \mu\text{m}$ , the spatial resolution of the CR system should be improved to  $43.8\ \mu\text{m}$  (Konica Minolta Regius 190), and the iodine density should be increased. Based on experimental results, the maximum magnification rate without blurring is approximately threefold using a  $100\text{-}\mu\text{m}$ -focus tube, and the rate increases with decreasing the focus diameter. In addition, the rate should be minimized to decrease the exposed dose from patients.

At a tube voltage of 60 kV and a current of 0.50 mA, the maximum number of photons was approximately  $4 \times 10^7$  photons/( $\text{cm}^2 \cdot \text{s}$ ) at 1.0 m from the source, and the photon count rate can be increased easily using a rotating anode microfocus tube. Recently, the maximum electric power of the microfocus x-ray tube has been increasing, and the kilowatt-range tube can be realized. Furthermore, since a  $10\text{-}\mu\text{m}$ -focus rotating anode tube has been developed by Hitachi Medical Corporation, dynamic high-resolution angiography is possible using a flat panel detector with a pixel size of less than  $100\ \mu\text{m}$ . Finally, this high-resolution, high-contrast angiography could be very useful for observing fine blood vessels in regenerative medicine, coronary arteries, and irregular capillaries in cancers.

#### Acknowledgments

This work was supported by Grants-in-Aid for Scientific Research (13470154, 13877114, 16591181, and 16591222) and Advanced Medical Scientific Research from MECSS, Health and Labor Sciences Research Grants (RAMT-nano-001, RHGTEFB-genome-005, and RHGTEFB-saisei-003), grants from the Keiryō Research Foundation, The Promotion and Mutual Aid Corporation for Private Schools of Japan, Japan Science and Technology Agency (JST), and the New Energy and Industrial Technology Development Organization (NEDO, Industrial Technology Research Grant Program in 2003).

#### References

1. R. Germer, "X-ray flash techniques," *J. Phys. E* 12, 336–350 (1979).
2. E. Sato, Y. Hayasi, R. Germer, E. Tanaka, H. Mori, T. Kawai, T. Ichimaru, S. Sato, K. Takayama, and H. Ido, "Portable x-ray generator utilizing a cerium-target radiation tube for angiography," *J. Electron Spectrosc. Relat. Phenom.* 137-140, 699–704 (2004).
3. E. Sato, E. Tanaka, H. Mori, T. Kawai, T. Ichimaru, S. Sato, K. Takayama, and H. Ido, "Demonstration of enhanced K-edge angiography using a cerium target x-ray generator," *Med. Phys.* 31, 3017–3021 (2004).
4. E. Sato, S. Kimura, S. Kawasaki, H. Isobe, K. Takahashi, Y. Tamakawa, and T. Yanagisawa, "Repetitive flash x-ray generator utilizing a simple diode with a new type of energy-selective function," *Rev. Sci. Instrum.* 61, 2343–2348 (1990).
5. A. Shikoda, E. Sato, M. Sagae, T. Oizumi, Y. Tamakawa, and T. Yanagisawa, "Repetitive flash x-ray generator having a high-durability diode driven by a two-cable-type line pulser," *Rev. Sci. Instrum.* 65, 850–856 (1994).
6. E. Sato, K. Takahashi, M. Sagae, S. Kimura, T. Oizumi, Y. Hayasi, Y. Tamakawa, and T. Yanagisawa, "Sub-kilohertz flash x-ray generator utilizing a glass-enclosed cold-cathode triode," *Med. Biol. Eng. Com-*

7. K. Takahashi, E. Sato, M. Sagae, T. Oizumi, Y. Tamakawa, and T. Yanagisawa, "Fundamental study on a long-duration flash x-ray generator with a surface-discharge triode," *Jpn. J. Appl. Phys., Part 1* 33, 4146–4151 (1994).
8. E. Sato, Y. Hayasi, R. Germer, E. Tanaka, H. Mori, T. Kawai, T. Ichimaru, K. Takayama, and H. Ido, "Quasi-monochromatic flash x-ray generator utilizing weakly ionized linear copper plasma," *Rev. Sci. Instrum.* 74, 5236–5240 (2003).
9. E. Sato, Y. Hayasi, R. Germer, E. Tanaka, H. Mori, T. Kawai, T. Ichimaru, S. Sato, K. Takayama, and H. Ido, "Sharp characteristic x-ray irradiation from weakly ionized linear plasma," *J. Electron Spectrosc. Relat. Phenom.* 137-140, 713–720 (2004).
10. E. Sato, E. Tanaka, H. Mori, T. Kawai, S. Sato, and K. Takayama, "Clean monochromatic x-ray irradiation from weakly ionized linear copper plasma," *Opt. Eng.* 44, 049002 (2005).
11. E. Sato, M. Sagae, E. Tanaka, Y. Hayasi, R. Germer, H. Mori, T. Kawai, T. Ichimaru, S. Sato, K. Takayama, and H. Ido, "Quasi-monochromatic flash x-ray generator utilizing a disk-cathode molybdenum tube," *Jpn. J. Appl. Phys., Part 1* 43, 7324–7328 (2004).
12. E. Sato, E. Tanaka, H. Mori, T. Kawai, T. Ichimaru, S. Sato, K. Takayama, and H. Ido, "Compact monochromatic flash x-ray generator utilizing a disk-cathode molybdenum tube," *Med. Phys.* 32, 49–54 (2005).
13. A. Momose, T. Takeda, Y. Itai, and K. Hirano, "Phase-contrast x-ray computed tomography for observing biological soft tissues," *Nat. Med.* 2, 473–475 (1996).
14. M. Ando, A. Maksimenko, H. Sugiyama, W. Pattanasiruwisawa, K. Hyodo, and C. Uyama, "A simple x-ray dark- and bright-field imaging using achromatic Laue optics," *Jpn. J. Appl. Phys., Part 2* 41, L1016–L1018 (2002).
15. H. Mori, K. Hyodo, E. Tanaka, M. U. Mohammed, A. Yamakawa, Y. Shinozaki, H. Nakazawa, Y. Tanaka, T. Sekka, Y. Iwata, S. Honda, K. Umetani, H. Ueki, T. Yokoyama, K. Tanioka, M. Kubota, H. Hosaka, N. Ishizawa, and M. Ando, "Small-vessel radiography in situ with monochromatic synchrotron radiation," *Radiology* 201, 173–177 (1996).
16. K. Hyodo, M. Ando, Y. Oku, S. Yamamoto, T. Takeda, Y. Itai, S. Ohtsuka, Y. Sugishita, and J. Tada, "Development of a two-dimensional imaging system for clinical applications of intravenous coronary angiography using intense synchrotron radiation produced by a multipole wiggler," *J. Synchrotron Radiat.* 5, 1123–1126 (1998).
17. E. Sato, K. Sato, T. Usuki, and Y. Tamakawa, "Film-less computed radiography system for high-speed imaging," *Ann. Rep. Iwate Med. Univ. Sch. Lib. Arts Sci.* 35, 13–23 (2000).
18. A. Ishisaka, H. Ohara, and C. Honda, "A new method of analyzing edge effect in phase contrast imaging with incoherent x-rays," *Opt. Rev.* 7, 566–572 (2000).
19. E. Sato, Y. Hayasi, R. Germer, E. Tanaka, H. Mori, T. Kawai, T. Ichimaru, S. Sato, K. Takayama, and H. Ido, "Portable x-ray generator utilizing a cerium-target radiation tube for angiography," *J. Electron Spectrosc. Relat. Phenom.* 137-140, 699–704 (2004).
20. E. Sato, E. Tanaka, H. Mori, T. Kawai, T. Ichimaru, S. Sato, K. Takayama, and H. Ido, "Demonstration of enhanced K-edge angiography using a cerium target x-ray generator," *Med. Phys.* 31, 3017–3021 (2004).

Eiichi Sato received his BS, MS, and PhD in applied physics from Tohoku Gakuin University, Sendai, Japan, in 1979, 1982, and 1987, respectively. He is currently a professor in the Department of Physics at Iwate Medical University. He has written some 400 publications and delivered some 200 international presentations concerning x-rays. His research interests include soft flash x-ray generators, quasi-x-ray laser generators, and high-speed radiography. In 2000, he received the Schardin Gold Medal from the German Physical Society, in 2003 he received the Takayama Award (Gold Medal) from the Japan Society of High Speed Photography and Photonics, and he received the Honorable Mention Poster Award from the SPIE International Symposium on Medical Imaging 2005.

Etsuro Tanaka received his MD and PhD degrees in medicine from Kumamoto University, Japan, in 1980 and 1986, respectively. He worked on medical image processing in the Department of Physiology, Tokai University, Japan, from 1988 to 2003. He is currently a professor in the Department of Nutritional Sciences, Tokyo University of Agriculture, Japan. His research interests include medical image processing, human physiology, and clinical nutrition.

**Hidezo Mori** received a medical degree from Keio University School of Medicine, Tokyo, Japan, in 1977, and also a PhD from the Post Graduate School, Keio University School of Medicine. Now he is the director of the Department of Cardiac Physiology at the National Cardiovascular Center, Suita, Japan. His primary research interests are regenerative therapy in cardiovascular disease, microcirculation, and medical applications of structural biology.

**Hiroki Kawakami** received BS and MS degrees in precision mechanics engineering from Shizuoka University in 1990 and 1992, respectively, and joined Hamamatsu Photonics K. K. in 1992. He was involved in a national project on the research and development of microangiography systems from 1999 to 2004. Now he is engaged in research and development of microfocus x-ray sources and high-resolution x-ray imaging systems.

**Toshiaki Kawai** received the BS degree in precision mechanics and the MS degree in electronic engineering from Shizuoka University, Hamamatsu, Japan, in 1964 and 1974, respectively. In 1974, he joined the Hamamatsu Photonics K. K., where he worked on the research and development of solid-state infrared detectors, and then from 1978 to 1981, he engaged in research work on the NEA cold cathode for application to imaging camera tubes. He is now the project coordinator of Electron Tube Division 2 and is engaged in the development and manufacturing of imaging devices and x-ray equipment. He is a member of the Japan Radioisotope Association and the Institute of Image Information and Television Engineers of Japan.

**Takashi Inoue** received his MD and PhD degrees in 2000 from Tohoku University. He is currently an assistant professor in the Department of Neurosurgery at Iwate Medical University, and a member of the Japan Neurosurgical Society. His research interests include neurosurgery and magnetic resonance imaging.

**Akira Ogawa** received his MD and PhD degrees in 1981 from Tohoku University. He is currently a professor in the Department of Neurosurgery, dean of the School of Medicine at Iwate Medical University, and is a trustee of the Japan Neurosurgical Society. His research interests include neurosurgery and cerebrovascular disease.

**Mitsuru Izumisawa** graduated from Iwate Medical University, School of Dentistry, in 1992. He worked for the Department of Oral Surgery at Iwate Medical University Hospital from 1992 to 1999. He received his MD degree from Iwate Medical University in 2004. As of 2005, he is an assistant professor in the Department of Oral Radiology. His research interests include diagnostic modality and intra-arterial infusion chemotherapy for head and neck cancer.

**Kiyomi Takahashi** received her MD degree from Iwate Medical University in 1989. She worked for the Department of Neurology, Johns Hopkins University School of Medicine from 1992 to 1994. She is currently an assistant professor in the Department of Microbiology, Iwate Medical University School of Medicine. Her research interests include pathophysiology of neurological involvement in HIV and Shiga toxin-producing *E. coli* (STEC) infections, and cerebral angiography.

**Shigehiro Sato** received his MD degree from Iwate Medical University in 1980. He worked for the laboratory of the Division of Pediatric Infectious Diseases at Johns Hopkins Hospital from 1985 to 1989. He is currently a professor in the Department of Microbiology at Iwate Medical University. His research interests include central nervous system damage caused by Vero toxin, a cell culture system for vaccine development, and microangiography.

**Kazuyoshi Takayama** received his BS degree from Nagoya Institute of Technology in 1962. In 1970, he received his PhD in mechanical engineering from Tohoku University. He is currently a director (professor) in the Shock Wave Research Center, Institute of Fluid Science at Tohoku University. His research interests include various shock wave phenomena, high-speed photography, and flash radiography. He has received seven awards, including the coveted Ernst Mach Medal in 2000.

**Jun Onagawa** received his BS and PhD degrees in applied physics from Tohoku Gakuin University in 1968 and 2001, respectively. He is currently a professor in the Department of Applied Physics and Informatics, Faculty of Engineering, at Tohoku Gakuin University. His research interests include target metallography and x-ray spectroscopy.

## Full Paper

**Edaravone Preserves Coronary Microvascular Endothelial Function After Ischemia/Reperfusion on the Beating Canine Heart In Vivo**Renan Sukmawan<sup>1,\*</sup>, Toyotaka Yada<sup>2</sup>, Eiji Toyota<sup>1</sup>, Yoji Neishi<sup>1</sup>, Teruyoshi Kume<sup>1</sup>, Yoshiro Shinozaki<sup>3</sup>, Hidezo Mori<sup>4</sup>, Yasuo Ogasawara<sup>2</sup>, Fumihiko Kajiya<sup>2</sup>, and Kiyoshi Yoshida<sup>1</sup><sup>1</sup>Departments of <sup>1</sup>Cardiology and <sup>2</sup>Medical Engineering and Systems Cardiology, Kawasaki Medical School, Kurashiki 701-0192, Japan<sup>3</sup>Department of Physiology, Tokai University School of Medicine, Isehara 259-1193, Japan<sup>4</sup>Department of Cardiac Physiology, National Cardiovascular Center Research Institute, Suita 565-8565, Japan

Received January 22, 2007; Accepted June 13, 2007

**Abstract.** We examined whether edaravone (3-methyl-1-phenyl-2-pyrazolin-5-one), a free radical scavenger, exerts its protective effect on coronary microvessels after ischemia/reperfusion (I/R) in vivo. Ninety-minute coronary occlusion followed by reperfusion was performed in 16 open-chest dogs with and without edaravone administration. Coronary small artery ( $\geq 100 \mu\text{m}$  in size) and arteriolar ( $< 100 \mu\text{m}$ ) vasodilation, in the presence of endothelium-dependent (acetylcholine) or -independent (papaverine) vasodilators, was directly observed using intravital microscopy before and after I/R. I/R impaired microvascular vasodilation in response to acetylcholine, whereas administration of edaravone preserved the response in microvessels of both sizes, but to a greater extent in the coronary small arteries. No significant changes were noted with papaverine administration. In the edaravone group, the fluorescent intensity from reactive oxygen species (ROS) was lower, whereas nitric oxide (NO) intensity was higher relative to controls in the microvessels of the ischemic area. In conclusion, edaravone preserves coronary microvascular endothelial function after I/R in vivo. These effects, which were NO-mediated, were attributed to the ROS scavenging properties of edaravone.

**Keywords:** coronary microvessel, edaravone, ischemia/reperfusion, reactive oxygen species, nitric oxide (NO)

**Introduction**

Coronary microvessels play a pivotal role in the regulation of coronary blood flow (1, 2). Dysfunction of coronary microvessels, especially the resistance vessels, has been associated with an increase in future cardiovascular events in patients with coronary diseases (3, 4). Even in normal subjects, coronary microvascular dysfunction has been shown to increase the risk for a cerebrovascular event (5).

Ischemia/reperfusion (I/R) may result in microvascular dysfunction that further attenuates cardiac func-

tional recovery (6–8). One of the central mechanisms responsible for the adverse effect of I/R is free radical production, which includes reactive oxygen species (ROS) (9, 10). A burst of ROS is generated during ischemia and in early reperfusion. This burst overwhelms the antioxidant defense band and causes disturbance in the cardiovascular system (11, 12).

Edaravone (3-methyl-1-phenyl-2-pyrazolin-5-one), a potent free radical scavenger, has been shown to protect cardiomyocytes and brain against I/R injury (13, 14). However, the beneficial effects on coronary microcirculation after I/R remains unknown. We sought to define the effects of edaravone on coronary microvessels after I/R in vivo by 1) direct observation of endothelium-dependent and -independent vasodilation of subepicardial coronary microvessels on the beating canine heart using a charged couple device (CCD) intravital microscope and 2) In-situ detection of ROS and

\*Corresponding author. Present address: Department of Cardiology and Vascular Medicine, University of Indonesia/National Cardiovascular Center, Jalan Letjen S. Parman Kav 87, Jakarta 11420, Indonesia. rey1708@yahoo.com

Published online in J-STAGE

doi: 10.1254/jphs.FP0070186



nitric oxide (NO) in coronary microvessels.

## Material and Methods

### *Animal preparation*

We conformed to the Guideline on Animal Experiments and the Guide for the Care and Use of Laboratory Animals published by the National Institutes of Health (NIH) of the United States and the Guiding Principles for the Care and Use of Laboratory Animals approved by the Japanese Pharmacological Society. Sixteen adult mongrel dogs of either sex (15–24 kg; purchased from Nagoyalab Service, Mizunami) were premedicated with ketamine (10 mg/kg, i.m.) and anesthetized with sodium pentobarbital (25 mg/kg, i.v.). Each animal was intubated and mechanically ventilated (model VS-600; Instrumental Development, Pittsburgh, PA, USA) with 2%–3% fluorethane. Blood gas and oxygen saturation were controlled within physiologic ranges throughout the experiment. Open-chest surgery was performed by medial sternotomy and the left anterior descending artery (LAD) was isolated free from surrounding tissue at proximal and medial portions. A transonic flow probe (T206; Transonic Systems, Ithaca, NY, USA) was placed at the medial portion of the LAD to measure the coronary flow rate. A clamp was placed at the proximal LAD to produce coronary occlusion and reperfusion. Visible native collateral vessels were ligated to limit collateral flow into the ischemic area during LAD occlusion. A 6F-catheter was inserted into the right carotid artery through the left coronary artery to administer the vasodilator.

### *Experimental protocols*

After instrumentation, a minimum of 30 min were allowed for stabilization while monitoring hemodynamic variables. The study protocol was as follows: i) The arteriolar vasodilatory response to endothelium-dependent (acetylcholine, 1  $\mu$ g/kg, i.c.; Daiichi Pharmaceutical Co., Ltd., Tokyo) and -independent (papaverine, 1 mg, i.c.; Dainippon Sumitomo Pharma Co., Ltd., Osaka) vasodilators were examined before and after coronary I (90 min)/R (60 min) under the following conditions: a) control condition, and b) edaravone administration (3 mg/kg, i.v.; supplied by Mitsubishi Pharma Co., Ltd., Osaka) before coronary occlusion. Microspheres were administered at 85 min of coronary occlusion to measure regional myocardial blood flow (MBF). ii) Fluorescent treatment to assess microvascular ROS and NO were performed in 6 dogs ( $n=3$ , each group) after a 60-min reperfusion period. iii) In another 10 dogs ( $n=5$ , each), reperfusion was continued for 5 h and the infarct size and regional MBF were measured.

### *Intravital CCD microscopy*

Direct observation of coronary microvascular vasodilation on the beating heart was performed by using a needle-probe intravital CCD microscope (VMS 1210; Nihon Kohden, Tokyo). It contains a gradient index lens (with a magnification of 200) surrounded by light guide fibers and a double lumen sheath. To avoid direct compression of the vessels by the needle-tip, a doughnut-shaped balloon had been installed (15). Vascular images were acquired by gently placing the needle-probe on subepicardial microvessels and were recorded at 30 frames/s. Off-line quantitative analysis was performed using an NIH image analysis software by measuring maximum diameter changes during acetylcholine or papaverine administration.

### *In situ detection of ROS and NO in coronary microvessels*

After reperfusion, the heart was immediately removed. The LAD orifice and left circumflex (LCX) artery were cannulated for a continuous phosphate-buffered saline (PBS) infusion. Small tissue blocks were taken from both ischemic (LAD area) and non-ischemic regions (LCX area), and they were frozen in optimal cutting temperature compound (Tissue-Tek; Sakura Fine Chemical, Tokyo) within a few hours. Fluorescent images of the microvessels were obtained using a fluorescent microscope (Olympus BX 51; Olympus, Tokyo). Dihydroethidium (DHE; Molecular Probes, Eugene, OR, USA) and 4,5-diaminofluorescein diacetate (DAF-2DA; Daiichi Pure Chemicals, Tokyo) were used to detect ROS and NO production, respectively (16). Five regions of interest (ROI) were selected within the intimal layer of each microvessel. Fluorescent intensities of ROS and NO in the microvessels were measured by NIH software. The average value of the peak fluorescent intensity from each ROI was divided by background intensity (relative intensity) and noted as the microvascular ROS or NO intensities.

### *Western blotting*

Myocardial tissue samples from the LAD and LCX area in each group were isolated for western blotting to assess endogenous NO synthase (eNOS) protein expression after I/R, as previously described (8, 16). Briefly, myocardial tissues were homogenized in the lysis buffer. After centrifugation, the supernatant was collected for immunoblotting. The proteins were transferred by semi-dry electroblotting to polyvinylidene difluoride membranes. The blots were then blocked and incubated with rabbit anti-eNOS polyclonal antibody (0.1  $\mu$ g/ml; Santa Cruz Biotechnology, Santa Cruz, CA, USA) or anti-actin antibody (Santa Cruz Biotechnology) for 120 min

at room temperature. The blots were then incubated with horseradish peroxidase-conjugated goat anti-rabbit IgG (0.08  $\mu\text{g}/\text{ml}$ ; Santa Cruz Biotechnology). The antibody was visualized using an enhanced chemiluminescence method (ECL; Amersham Biosciences, Piscataway, NJ, USA). The integrated density of the eNOS bands was normalized by actin band density (relative density) (NIH Image).

#### Regional blood flow and infarct size

To confirm infarct size reduction by edaravone in relation to the effect of collateral flow, regional MBF was assessed by non-radioactive microspheres (Sekisui Plastic Co., Ltd., Tokyo), as previously described (17). Briefly, 1 ml of the microsphere suspension ( $2$  to  $4 \times 10^6$  spheres) was injected into the left atrium 85 min after the onset of coronary occlusion. MBF was measured by assessing X-ray spectra of the fluorescent stable heavy elements using a wavelength-dispersive spectrometer (model PW 1480; Philips Co., Ltd., Eindhoven, the Netherlands). Myocardial collateral flow (ml/min per gram) was calculated using the following formula: tissue flow-rate = tissue counts  $\times$  (reference flow / reference counts).

Myocardial short-axis slices (5-mm-thickness) of the left ventricle were made and incubated in 1% 2,3,5-triphenyltetrazoliumchloride solution (Sigma, Tokyo) for 10 min to identify the infarct area. Infarct size was expressed as a percentage of the infarct area relative to the area of risk (18).

#### Statistical analysis

Data are expressed as the mean  $\pm$  S.E.M. The vascular response was analyzed by one-way analysis of variance followed by a Scheffe's post-hoc test for multiple comparisons (Figs. 1C, 2, 3, and 4). Regression analysis was applied in Fig. 5. Statistical significance was defined as  $P < 0.05$ .

## Results

#### Hemodynamics

Hemodynamic data are shown in Table 1. Mean arterial pressure and heart rate during administration of acetylcholine and papaverine were not statistically different as compared to their respective baseline. Hemodynamic variables at baseline did not significantly change before and after I/R nor after edaravone administration.

#### Endothelium-dependent vasodilation

We assessed the diameter changes of 22 coronary microvessels under acetylcholine (1  $\mu\text{g}/\text{kg}$ , i.c.) in each group. The diameter changes of small artery and arteriole in each group are depicted in Fig. 1, A and B. Under control conditions (without edaravone), I/R strikingly impaired endothelium-dependent vasodilation at 60 min after I/R. Meanwhile, edaravone administration augmented the response in coronary microvessels of both sizes. Preservation of vasodilation under acetylcholine was more prominent in the small artery than the arteriole. Coronary flow in the presence of acetylcholine was improved after I/R in the edaravone-administered group compared with that in the controls (without edaravone) (Fig. 1C).

#### ROS intensity in coronary microvessels

Fifteen coronary microvessels ( $< 300 \mu\text{m}$ ) were assessed from both the LAD and LCX areas in both groups (Fig. 2). ROS fluorescent intensity at 60 min after I/R in the microvessels from the LAD area in the control group was higher than in the LCX area ( $P < 0.01$ ). Meanwhile, ROS intensity in the microvessels from the LAD area of the edaravone group was significantly lower than that in the control group ( $P < 0.01$ ).

#### Intensity of NO in coronary microvessels

Fluorescent intensity of NO in the endothelial layer was assessed semi-quantitatively in 15 microvessels from the LAD or LCX areas in both groups 60 min after

Table 1. Hemodynamics data before and after ischemia/reperfusion

	Before I/R			After I/R		
	Baseline	Acetylcholine	Papaverine	Baseline	Acetylcholine	Papaverine
Mean blood pressure (mmHg)						
Control	91 $\pm$ 4	90 $\pm$ 6	91 $\pm$ 4	89 $\pm$ 4	89 $\pm$ 5	87 $\pm$ 5
Edaravone	92 $\pm$ 2	91 $\pm$ 4	90 $\pm$ 3	93 $\pm$ 3	91 $\pm$ 5	90 $\pm$ 4
Heart rate (beats/min)						
Control	123 $\pm$ 5	125 $\pm$ 3	126 $\pm$ 4	120 $\pm$ 4	122 $\pm$ 5	120 $\pm$ 5
Edaravone	124 $\pm$ 4	126 $\pm$ 6	123 $\pm$ 5	123 $\pm$ 4	121 $\pm$ 5	120 $\pm$ 4

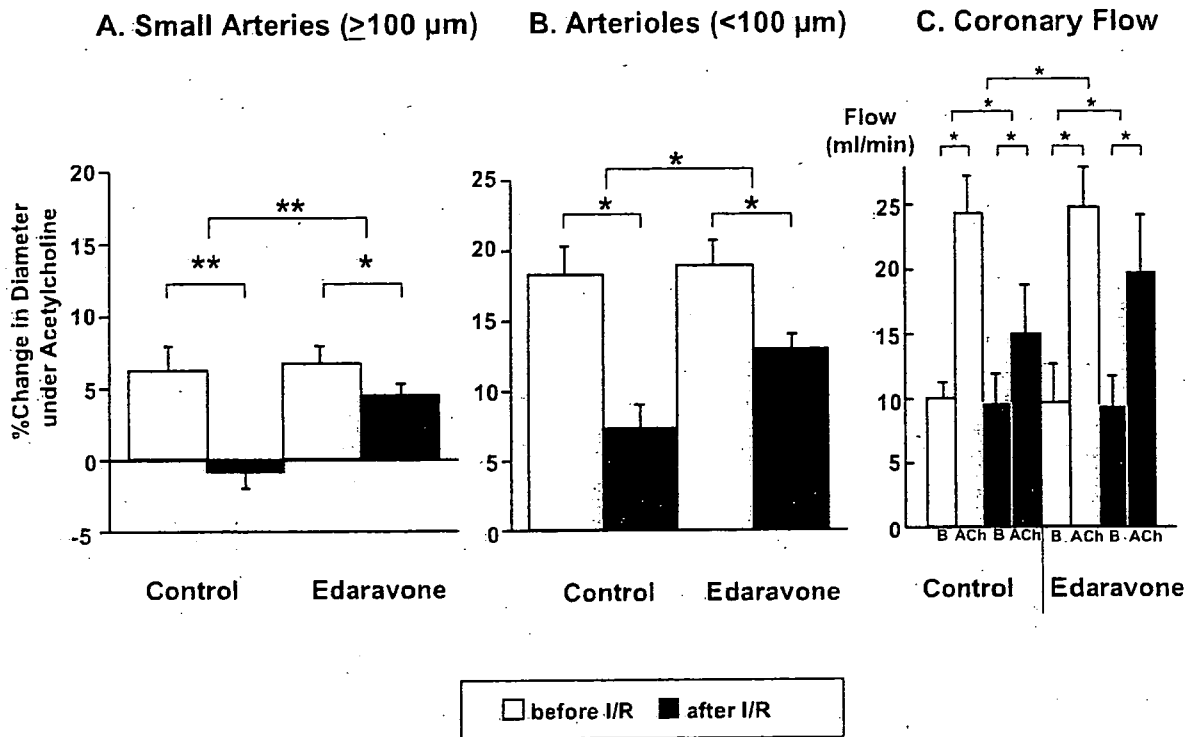


Fig. 1. Endothelium-dependent vasodilation in coronary microvessels in vivo. Edaravone administration augmented the vasodilation of small arteries (A) and arterioles (B) and improved coronary flow (C) under acetylcholine after I/R. Number of small arteries and arterioles assessed were 10 and 12, respectively. \* $P < 0.05$ , \*\* $P < 0.01$ . B = baseline, ACh = acetylcholine.

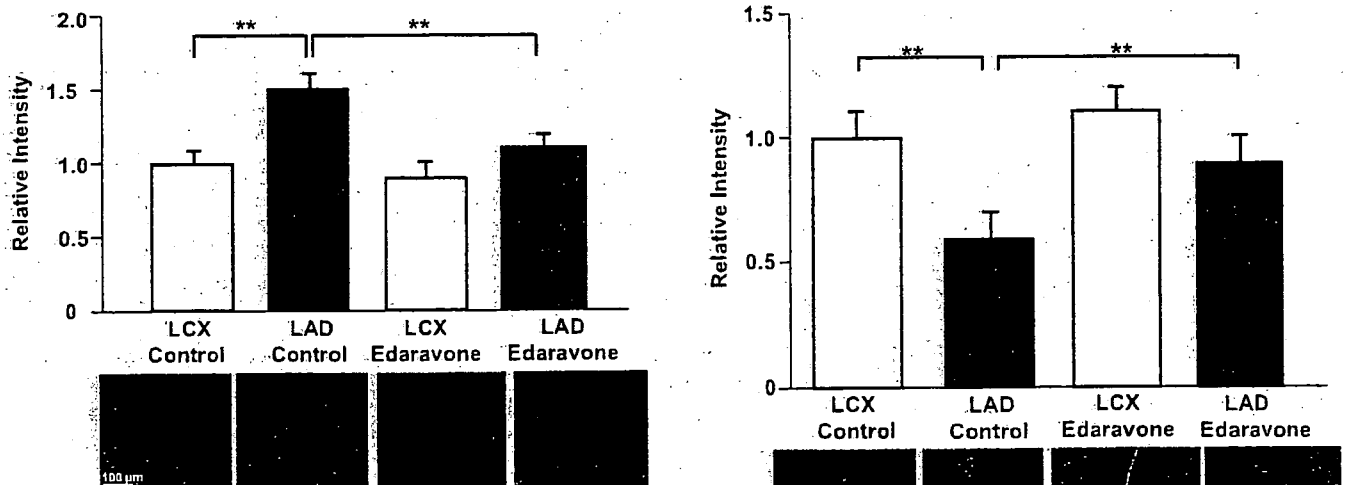


Fig. 2. In situ detection of ROS in coronary microvessels after I/R. The fluorescent intensity of ROS in microvessels from each area is shown ( $n = 15$ , in each area) with their representative DHE-fluorescence image of ROS in the vessels. \*\* $P < 0.01$ .

I/R (Fig. 3). In the LAD area of the control group (without edaravone), I/R reduced the microvascular NO intensity level as compared to the LCX area ( $P < 0.01$ ). Administration of edaravone significantly preserved NO

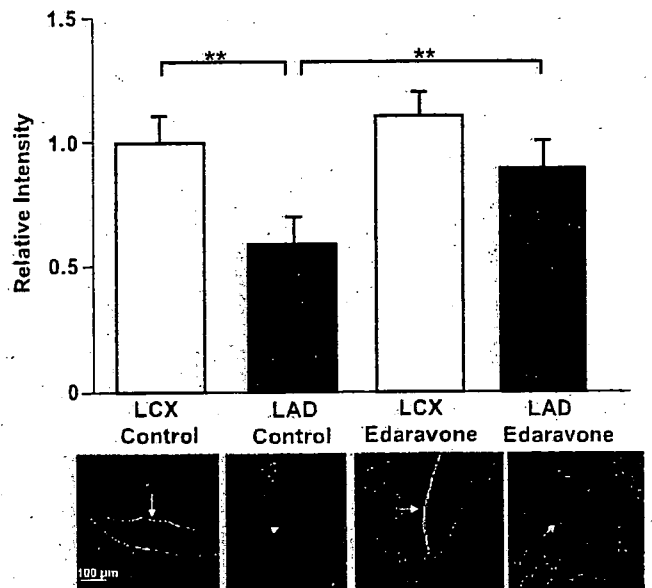


Fig. 3. In situ detection of NO in coronary microvessels after I/R. Fluorescent intensity of NO in microvessels from each area is shown ( $n = 15$ , in each area) with their representative DAF2-DA fluorescence image of NO in the endothelial layer (white arrow). \*\* $P < 0.01$ .

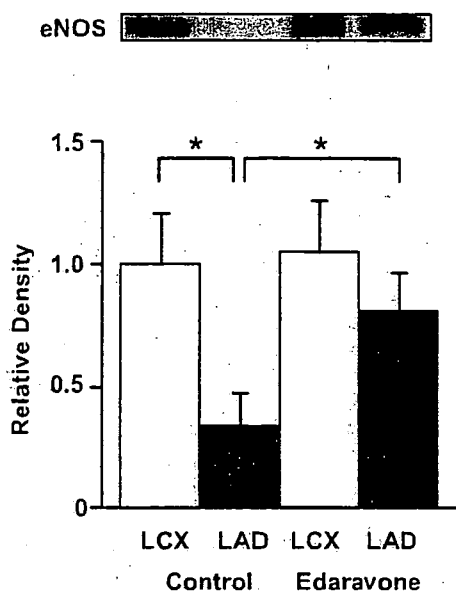


Fig. 4. eNOS protein immunoblotting after I/R. Edaravone administration augmented myocardial eNOS expression after I/R in the ischemic area. \* $P < 0.05$ .

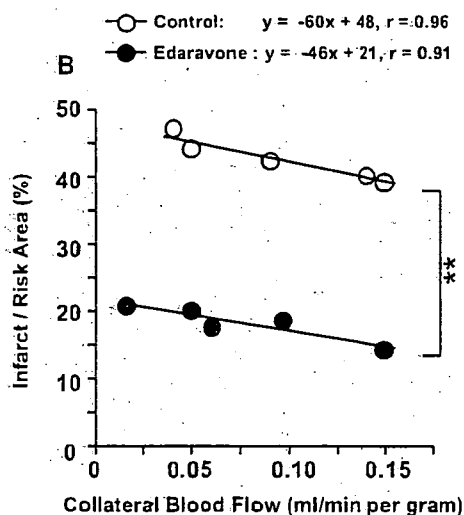


Fig. 5. Correlation of regional collateral flow and infarct size in the control and edaravone groups. \*\* $P < 0.01$ .

fluorescent intensity in microvessels of LAD relative to the control group ( $P < 0.01$ ).

#### Myocardial eNOS expression

Myocardial eNOS protein expression in the LAD distribution after I/R was significantly decreased relative to the LCX area in the control group (without edaravone,  $P < 0.05$ , Fig. 4). Edaravone augmented eNOS protein expression in the LAD area ( $P < 0.05$  vs controls).

#### Collateral flow and infarct size

There were linear negative correlations between regional collateral MBF and infarct size in the control ( $y = -60X + 48$ ,  $r = 0.96$ ,  $P < 0.001$ ) and edaravone ( $y = -46X + 21$ ,  $r = 0.91$ ,  $P < 0.001$ ) groups, which were significantly different between the 2 groups ( $P < 0.01$ , Fig. 5). This finding indicated that the protective effect of edaravone was independent of collateral flow.

#### Endothelium-independent vasodilation

Endothelium-independent vasodilation with papaverine (1 mg, i.c.) was comparable under all conditions (Fig. 6). Administration of edaravone did not result in any significant diameter changes in small arteries and arterioles under papaverine after I/R.

#### Discussion

The present study revealed that edaravone preserves endothelium-dependent vasodilation in coronary small arteries and arterioles after I/R injury on the beating canine heart in vivo by reducing ROS and thereby augmenting NO availability in the microvessels. To our knowledge, the present study is the first to report that edaravone exerts protective effects on the coronary microvascular endothelial function after I/R on the beating heart in vivo.

#### Scavenging ROS by edaravone during ischemia/reperfusion

Generation of ROS during I/R has been shown through several mechanisms such as the xanthine oxidase, mitochondrial electron transport chain, and NADPH oxidase pathways (10). In the present study, we revealed that edaravone scavenged ROS generated in coronary microvessels during I/R (Fig. 2). Previous studies have shown other beneficial effects of edaravone such as inhibition of the production of superoxide anion on the infarct rim (14), suppression of lipid peroxidation products (19), and reduction in inflammatory changes (20).

The burst of vascular ROS production following I/R led to endothelial dysfunction, which may have occurred as a result of hypoxic injury, manifested by endothelial cell swelling that results in the no reflow phenomenon within the first minutes of reperfusion (21). The ROS may also rapidly react with NO to form a toxic peroxynitric radical (i.e., ONOO<sup>-</sup>) that further increases free radical accumulation resulting in endothelial injury (9). If the ischemia lasts for hours, structural changes such as edematous mitochondria in endothelial and smooth muscle cells, microvilli formation on the surface of endothelial cells, and increased pinocytotic activity and